Journal of Environmental Science and Engineering A 6 (2016) 298-311
doi:10.17265/2162-5298/2016.06.004

Numerical Heat Transfer Modelling for Rapid Impact Assessment of Limiting Thermostat Reliability on Fuel-Oil Burner Pre-Heaters: A Case Study

Barış Elbüken

Heating Division, Alarko Carrier Research and Development Center, GOSB, Gebze 41480, Kocaeli, Turkey

Abstract: In this paper, the impact of limiting thermostat on the rupture event occuring in Fuel-Oil burner fuel pre-heaters' resistant (heat generating) wires is inspected numerically. Gaseous fuel content in the pipeline has also been issued as a possibility. Heater's inner temperature distributions have been simulated by an in-house MATrix LABoratory (MATLAB®) script in order to understand the resistant wire exposure to high temperatures by numerous scenarios. It is concluded that the effect of fuel flowrate is not a major effect on the wires' fate because of the limiting thermostat co-working. The main difference between the calculations is the effect of thermostat cut off function. The numerical simulations enlightened the dominant effect of thermostat sensing delay, so the overheating event. Intolerable delay results with a quick drop in the thermal efficiency and an increased possibility on wire rupture due to overheating which means a burner malfunction. Referring to the first numerical simulation results, a distributed and reduced heat flux was implemented with the same fluid and thermodynamic properties on a revised pre-heater model with an increased heater plate. The increment, thus the reduction on the heat flux of the ribbon wires has been noted as the key for safe operation.

Key words: Fuel oil burner, numerical simulations, resistant wires rupture, thermostat delay.

Nomenclature

c_p	specific heat for constant pressure,	$J/(kg°K)$
$c_{v\text{-}gas}$	specific heat for constant volume,	$J/(kg°K)$
e'	heat energy production per unit length,	W/m
g	standard earth gravity,	m/s^2
h_i	coefficient of convection for i,,	$W/(m^2.{}^oK)$
k_i	coefficient of conduction for i,	$W/(m.{}^oK)$
$\dot{m}$	mass flowrate,	kg/s
$\dot{n}$	molar flowrate,	mol/s
$\dot{p}$	heat flux by convection,	W
$\dot{p}''$	heat flowrate per unit area,	W/m^2
t	time,	s
v	velocity of fuel inside the pipe stages,	m/s
w	molar mass of the fuel,	kg/s
$\%m_{ev}$	predicted gaseous fuel content pumped through the pre-heater	-
A_i	area of i,	m^2
B	flow regulating magnification factor,	-
D_H	hydraulic diameter,	m
Gr	Grashof number,	-
N_A	Avogadro's constant,	-
N_p	Number of heater plates,	-
Nu	Nusselt number,	-
Pr	Prandtl number,	-
Q_{LH}	latent heat of vaporization for fuel-oil,	W
T_i	temperature of i,	${}^oC, {}^oK$
U	effective (useful) power,	W
X_i	thickness of layer i,	m
ΔS_{ev}	entropy of evaporation,	$W/{}^oK$
ΔT_i	temperature difference at or between i,	${}^oC, {}^oK$
β	coefficient of volumetric expansion,	${}^oK^{-1}$
μ	dynamic viscosity,	$kg/(m.s)$
η_t	thermal efficiency,	-
ρ	mass density,	kg/m^3

Corresponding author: Barış Elbüken, M.Sc., B.Sc. B.Sc., R&D engineer, research fields: numerical simulations, heat transfer, reactive flows, aeroacoustics, VIV, internal flows of non-Newtonian fluids.

1. Introduction

The pre-heaters used in the Fuel-Oil burners are devices responsible for decreasing the viscosity of the fuel to be injected towards the injectors to appropriate values by transferring heat energy to the flowing fuel. The inspected device in this paper consists of three sandwich layers assembled adjacently from the fuel

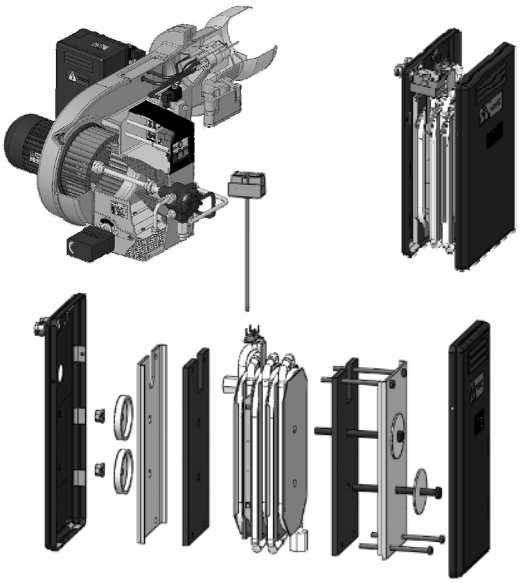

Fig. 1 Fuel-Oil burner, the pre-heater and the model assembly with sub-components.

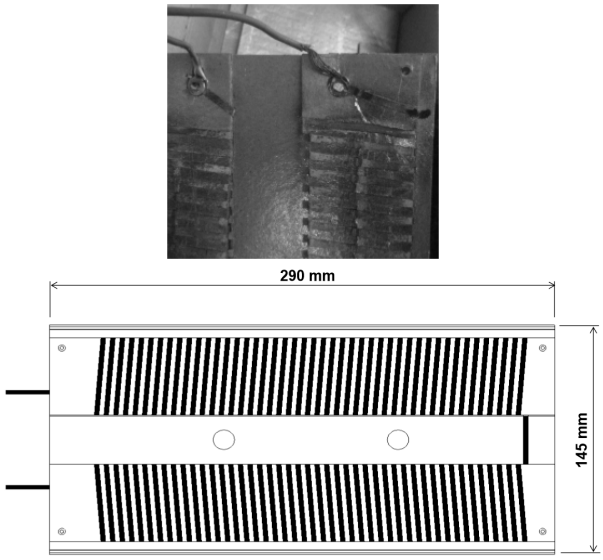

Fig. 2 Sample image for a ruptured heater plate and the wire windings in the 3.5 kW heater plate.

inlet side towards the heater exit. Every layer has a steel sheet commonly shared between the pairs. The sandwich layer is made up of fuel coils and a heater plate assembly between them. Two joining central bolts and nuts with wide washers and four tightening bolts and nuts are responsible for holding all the components still with two additional high insulator (adiabatic wall) plates at both ends of the assembly. All the three heater plates have an electrical heat production of 3.5 kW which gives a total load of 10.5 kW.

Some reasons for overheating the ribbon shaped resistance wires—whose thickness is 0.3 mm—above the maximum temperature of operation (1,300 ^{o}C) will probably result in a tear or damage on the ribbons [1]. An example of rupture on the ribbons was shown in Fig. 2.

Major variations (poor quality of the fuels in the market) in the physical properties of the No. 4 Fuel-Oil in Turkey may be a primer cause for the resistant wires' rupture phenomenon in the heavy oil pre-heaters. Regarding to the MSDS documents of No. 4 Fuel-Oil, the fuel has a boiling temperature of 177 ^{o}C in minimum and a maximum of 371 ^{o}C [2]. Various documentations about Fuel-Oils and heavy Fuel-Oils tend to be between nearly 170 ^{o}C and 650 ^{o}C [3].

The burner's fuel pump which is responsible for conveying the fluid Fuel-Oil through the pre-heater to the injectors depends functionally on the fuel's viscosity which is also a function of the fuel temperature passing by the pump's gears. Thus the boiling point can also be taken into account as a corrolative property with the fuel viscosity.

The operating thermostat is thought to be responsible for the second main reason for the wire rupture. The thermostat is in a linear dry-contact with three objects: a heater plate, a fuel carrying coil and an acordeon spring which is a poor heat sensing construction with low sensitivity. Damage or malfunction of the operating thermostats in the field applications was in common with resistant wires' rupture phenomenon with high coherence.

The heat generated may poorly be transferred to the fuel so that the wires being subjected to excess heat resulted in a mass decrease of the convective heat transfer coefficient, leading to the rupture. The generated heat flux is 83.6 kW/m^2 for the resistant ribbon wires in operation in the upper formation. It is nearly a guarantee for damage if the core temperature of the wires reaches the maximum operating limit of 1,300 ^{o}C [1]. The link for the wire specs can be found at the references section.

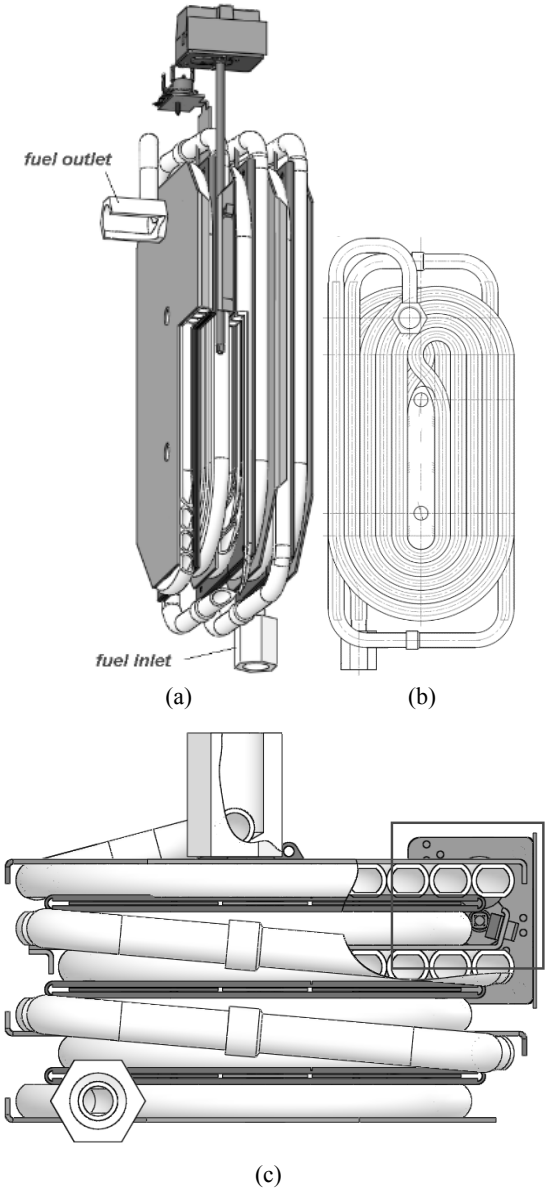

Fig. 3 (a) Physical model for calculations; (b) coil piping; (c) bottom view and thermostat contact environment (denoted in a rectangle).

The molar weight for No. 4 Fuel-Oil has been assumed as 347 g/mol regarding a weighted distribution of massive hydrocarbons [4, 5]. By the aid of Kistiakowsky equation [6], the latent heat of vaporisation for the fuel has been tried to be calculated. Different problem scenarios depending on different boiling point variations have formerly been calculated and figured by Elbüken which was the result of an analytical calculation. As a product, a boiling start position versus fuel boiling point diagram has been generated. This calculation has been made on a linear stepwise temperature increase basis towards the exit coil with the assumption about the ability of boiling. Depending on the impossibility of determining the triple point and the critical point for the so called fuel because of high deviations in its content, boiling has been assumed to be a possible event in the analytical calculations [7].

After triumphing the analytical solution effort, a dimensional, transient and segregated in-house flow + heat transfer code has been written in MATLAB® for examining the system limiting thermostat's behavior and the time dependent correct heat distribution omitting the possibility of boiling due to fuel heating at 20 bar. Analytical results make one to focus on fuel viscosity and boiling point. In the contrary, various numerical simulations have enlightened the destructive effect of the delay in thermostat sensing. Fuel evaporation due to overheating can not be the primary reason for wire rupture. The m file of the code can be downloaded via the link in Ref. [8].

Boiling point, kinematic viscosity and density may be counted as the main physical properties of the fuel to be taken into account which could easily affect the heat distribution. It is also noted in spectacular documents about Fuel-Oil that, a vaporized mass percentage is also an experimental expectance so that this percentage has also been adopted to fuel flowrate tuning for the numerical simulations.

2. Materials

2.1 Problem Definition and Boundary Conditions

The physical structure of the heater has been modeled as an adjacent stepwise heater within every stage. The fuel is conveyed from the first stage through the last travels and carries heat towards the following stage also with stealing heat from the resistant wires; thus the fuel flow + heater wires' energy generation is in a direct competition defining the fuels fate, so does the wires'.

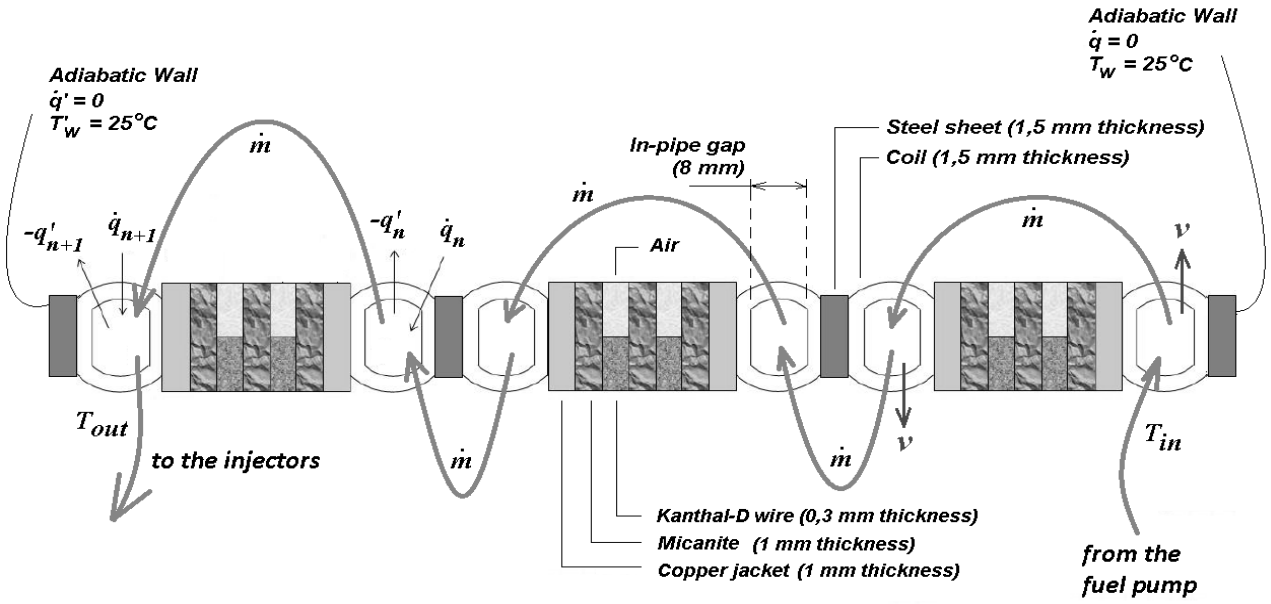

Fig. 4 Linear mathematical model and boundary conditions.

$$\dot{q}_i'' = \frac{\dot{q}_i}{A_i} = k_i \frac{\Delta T_i}{X_i} \tag{1a}$$

$$\dot{p}'' = \frac{\dot{p}}{A} = h\Delta T \tag{1b}$$

$$\Delta T = T_{out} - T_{in} \tag{2}$$

$$R_{res})_{(liquid,gas)} = \left\{\sum_{i=4} \frac{X_i}{k_i A}\right\} + \left.\frac{X_1}{k_1 A_1 + k_2 A_2}\right|_{\substack{wire,\\ air}} + \left.\frac{1}{h_{(liquid,gas)} A}\right|_{fuel} \tag{3a}$$

$$A = A_{1-(wire)} + A_{2-(air)} \tag{3b}$$

$$\dot{q}_{liquid,gas} = \begin{cases} \dfrac{1}{2N_p \psi} \left| \dot{m} c_{v-gas} (T_{out} - T_{boil}) \right|_{fuel} \\ \dfrac{1}{2N_p (1-\psi)} \left| \dot{m} c_{v-gas} (T_{out} - T_{boil}) \right|_{fuel} \end{cases} \tag{4}$$

$$\dot{q}_{LH} = \dot{n} Q_{LH} = \frac{\dot{m}}{w.N_A} Q_{LH} \tag{5}$$

$$Q_{LH}(T_{boil}) = T_{boil} \Delta S_{ev} = T_{boil}(36{,}6 + 8{,}31 \cdot \ln T_{boil}).10^{-3} [kJ.mol^{-1}] \tag{6}$$

$$\dot{q}_{liquid} + \dot{q}_{gas} + \dot{q}_{LH} = \eta_t .10{,}5[kW] \cong 7{,}7[kW] \tag{7}$$

$$T_{wire})_{(liquid,gas)} = < T >_{(liquid,gas)} - \frac{1}{12} \dot{q}_{(liquid,gas)} \left. \frac{X_4}{k_4 A} \right)_{micanite} = < T >_{(liquid,gas)} - \frac{1}{12} \dot{q}_{(liquid,gas)} R_4)_{micanite} \tag{8}$$

Here ψ is the free curvilinear path length in the pipe from the inlet to the starting of the boiling event as a percentage of total and N_p is the number of plates that is occupied in the heater assembly. The Kistiakowsky equation has been a tool for producing a sight for the evaporation energy in the analytical model: Eq. (6). The subscripts ($_{liquid}$ & $_{gas}$) states whether the equation's region of use (from pre-heater inlet to the boiling point or from the boiling point to the outlet of the device). The subscript ($_{LH}$) is for latent heat of evaporation and ($_{res}$) for resultant. The temperature notation between the brackets <*T*> is denoting the central temperature value which belongs to the plane of symmetry for the model. (*w*) is the average molar mass of the fuel (347 g/mol), (η) is the thermal efficiency of the heater depending on former experiments (~ 74%), ($\dot{n}$) is the molar flowrate and N_A is the Avogadro's number. T_{in}, T_{out} and T_{boil} are the

fuel temperatures at the heater inlet, outlet and boiling point in order.

The coefficient of convective heat transfer is a highly important parameter which has a big possibility of determining the occurence of the so called rupture phenomenon. Thus the calculation of the convective heat transfer coefficient has been made depending on the Nusselt thermal boundary layer theory with the following Eqs. (9a)-(9c) [9]:

$$Gr = \frac{1}{\mu^2} D_H^3 \rho^2 g \beta (\Delta T)_\delta \tag{9a}$$

$$\Pr = \frac{\mu c_p}{k} \tag{9b}$$

$$\frac{hD_H}{k} = Nu = a(Gr.\Pr)^m \tag{9c}$$

D_H is the hydraulic diameter of the piping coils, (β) is the volumetric thermal expansion coefficient, "μ" is the kinematic viscosity, a and b are model constants which is chosen in order to best define the thermal boundary flow and its orientation with the event geometry. The products are the well known Grashof Number (Gr), Prandtl Number (Pr) and the Nusselt Number (Nu), with k denoting the coefficient of thermal conduction for the fuel and h denoting the convective heat transfer coefficient needed for the numerical simulations. $(\Delta T)_\delta$ is the temperature difference between the wall and the boundary layer.

The heat transfer model is based on the following heat transfer coefficients for conduction and the specific heat for the Fuel-Oil given in Table 1.

In order to use the Kistiakowsky equation, it was neccesary to determine the average molecular weight for the heat absorbed while phase changes. Table 2 is the content for atmospheric residue heavy Fuel-Oils from the report of the American Petroleum Institute (API) submitted to the United States Environmental Protection Agency (US EPA) which also includes the vapour pressures of each type of species [4].

Referring to Table 2, it is obvious to mention that, predicting the molecular weight to be constant for Fuel-Oil distillates of different origins is not healthy but also can be stated that, weighted average of hydrocarbon compounds in the content gives a clear reference on molecular weight.

The molecular average weight of No. 4 Fuel-Oil has been taken as 347 g/mol with reference to the same report of API [4].

The mathematical model gives an important sight for the wire overheating situation whether in case of fuel evaporation would be possible. It should be noted that the mathematical model does not consist the thermostat cut-off function as it is posed in the previous pages so that, the results posed in the following pages are also beneficiary outcomes of the numerical solution. To be suspicious, depending on the critical or the triple points of the fuel content, a possible occurence of vaporised fuel flow would also be noted as a reason for wire rupture.

Depending on the fuel hydrocarbon content and the fuel pumping pressure, the ability of conveying the fuel through the circuit towards the injectors may seriously be affected by the fuel temperature passed by the fuel pump's gears. Whether depending on a malfunction of fuel depot thermostat or any kind of reason to increase the fuel inlet temperature may have a strong effect on the possibility of wire rupture.

Table 1 Heat transfer parameters for the model materials.

Material	Where used	Parameter	Value	Unit
St-38	Coil pipes + common steel sheets	k (*)	76	*W/(m°K)*
Copper	Heater plate outer cover	k	401	*W/(m°K)*
Kanthal-D	Resistant wires	k	11	*W/(m°K)*
Micanite	Heater plate inner layers	k	0,71	*W/(m°K)*
Air	-	k	0,024	*W/(m°K)*
Fuel-Oil (No:4)	15.5 °C	c_v (**)	1758.45	*J/(kg°K)*

(*) Coefficient of conduction , (**) Specific heat per unit mass for constant volume.

Table 2 Chemical composition and the vapour pressures for different type of hydrocarbon groups in Heavy Fuel-Oil [4, 5].

Chemical	Number of Carbon Atoms	Calculated Vapor Pressure for 25 °C, [Pa]	Chemical	Number of Carbon Atoms	Calculated Vapor Pressure for 25 °C, [*Pa*]
n-ALKANES	7	6×10^{3}	ISO-ALKANES	7	9×10^{3}
	11	5×10^{1}		11	8×10^{1}
	20	6×10^{-4}		20	6×10^{-4}
	50	2×10^{-7}		50	2×10^{-7}
CYCLO-ALKANES			POLAR/HETEROCYCLIC COMPOUNDS		
1-ring	7	6×10^{3}	• *Quinolines*		
	11	5×10^{1}	quinoline	9	8
	20	2×10^{-2}	4-pentylquinoline	14	2×10^{-2}
	50	2×10^{-13}	3-butyl-4-propyl-		
2-ring	11	9×10^{1}	5-butyl-quinoline	20	1×10^{-4}
	20	2×10^{-2}	4-hentetracontyl-quinoline	50	9×10^{-16}
	50	2×10^{-13}	• *Pyridines*		
3-ring	12	3×10^{1}	2-ethyl-pyridine	7	650
	20	2×10^{-2}	2-nonyl-pyridine	14	2×10^{-1}
	50	2×10^{-13}	2-pentadecyl-pyridine	20	8×10^{-4}
OLEFINS			2-pentatetracontyl-pyridine	50	2×10^{-16}
	7	8×10^{3}	• *Carboxylic acids*		
	11	1×10^{2}	cyclopenthane-3-methyl-1-		
	20	4×10^{-1}	carboxylic acid	7	7.6
	50	3×10^{-13}	[4.3.0]bicyclononane-5-		
AROMATICS			methyl-1-carboxylic acid	11	8×10^{-2}
1-ring	7	4×10^{3}	[4.2.4]tricyclotetradecane-11-		
	11	6×10^{1}	methyl-1-pentanoic acid	20	4×10^{-5}
	20	3×10^{-3}	[4.2.4]tricyclodecane-7-		
	50	2×10^{-14}	eicosyl-1-decacarboxylic acid	50	3×10^{-16}
2-ring	11	7	• *Thiophenes/benzothiophenes*		
	20	7×10^{-4}	2-propyl thiophene	7	370
	50	3×10^{-5}	dibenzothiophene	12	3×10^{-2}
3-ring	14	4×10^{-4}	dibenzothiophene 4,6-dibutyl	20	1×10^{-5}
	20	1×10^{-4}	dibenzothiophene 4,6-didecanyl	50	5×10^{-17}
	50	5×10^{-16}			

Regarding to this information, likewise the mass percentage to be evaporated, the percentage of pumping ability has also been adapted to the numerical model by polynomial curvefitting. By using the viscosity relation to fuel temperature, the fuel pump's capacity curve [10, 11] values has been transformed into a mass flowrate percentage versus fuel temperature graph for different pump pressures.

The vapour pressures of each species type is much more small compared with the pump operating pressure of 20 bar (Table 2). Thus for the numerical simulations, boiling of the flowing fuel was an omitted possibility and has been excluded from the model. This postulate can also be supported by using the Gay-Lussac's principle for comparing the predicted vapour pressures of each type of species depending on temperature. The maximum vapour pressure at 25 ^{o}C belongs to 7 carboned iso-alkene (C_7H_{16}—Heptane) is 9,000 Pa which is shown in Table 2. Even reaching the maximum operational limits of the resistant wire (1,300 ^{o}C) the pressure multiplier would be no more than 5.3 thus, 20 bar of pumping pressure would be high enough to keep the molecules in their liquid phase.

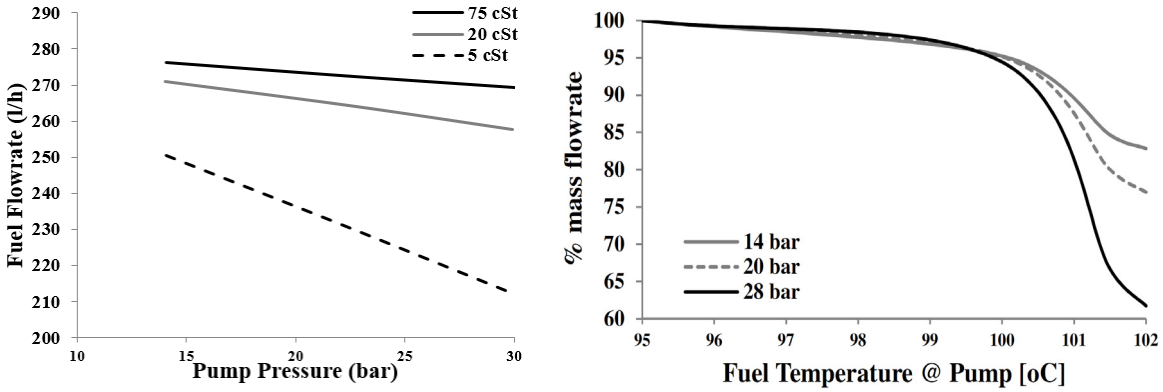

(a) (b)

Fig. 5 (a) Burner fuel pump's capacity curves [12]; (b) % pumping ability depending on fuel temperature [7].

Table 3 Examples about possible weighted formations of No:4 Fuel-Oil content [12].

	Species 1	Molecular weight	Species 2 (if exist)	Molecular weight	Total average
1	$C_{12}H_{26}$ n-Dodecane	17,033 g/mol	$C_{13}H_{28}$ n-Tridecane	18,436 g/mol	35,469 g/mol
2	$C_{20}H_{42}$ n-Eicosane	28,255 g/mol	C_5H_{12} n-Pentane	7,215 g/mol	35,470 g/mol

2.2 Numerical Solution Strategy

The heat generated by the resistant wires, as well as the heat transfered between the nodes of the linear mathematical model of the pre-heater device and the convective heat transfered through/from the fuel, has been modeled by an implicit (unconditionally stable) one dimensional transient and segregated code which takes fluid mass transfer (incompressible continuity equation) also into account. Thus the momentum equations are excluded from the solution for the ease of adaptation, increased codewriting speed and the structure of the single dimensional spatial domain.

$$\frac{\partial v}{\partial x} = 0 \tag{11}$$

$$\frac{\partial T}{\partial t} = k\frac{\partial^2 T}{\partial x^2} + e' \tag{12}$$

$$\%m_{ev} = (-0{,}14 + 0{,}013.T)\sqrt{\frac{t}{60}} \tag{13}$$

Above are the Eqs. of continuity for incompressible flow [13], one dimensional and transient heat conduction equation with heat generation [14, 15] and the predicted mass percentage for the naturally evaporated fuel content with reference to the EPA/600/R-03/072 technical report of the United States Environmental Protection Agency, National Exposure Research Laboratory [3]. Here v is for the one dimensional conservative velocity field which is normal to the span of the linear domain (through outwards or inwards) representing the fluid flow from a pipe coil stage to the following. T is for nodal temperature, e' is for the heat generation power per unit length and t for time in seconds.

The Eq. of continuity is adapted to the simulation by means of information transfer towards the following pipe coil stage at the appropriate timestep corresponding the fuel flowrate explicitly by forward time marching with centering in space. Assuming adiabatic and incompressible flow, the modified Bernoulli equation by the first law of thermodynamics can be used to show the temperature prediction of the n^{th} coil stage during the segregated mass transfer step of the algorithm.

$$T_n^{i+1} = T_n^i + \frac{1}{B}(T_{n+1}^i - T_{n-1}^i) \tag{14}$$

B is a magnification constant depending on the timestep size which is responsible for regulating the flow transfer to the adjacent pipe layer with respect to the fuel flowrate. The effect of B can better be

understood in the results section on the saw tooth profile of the displayed values. The discretization techniques for the heat equation can be found in numerous textbooks about numerical methods so that we directly give the equations for Euler implicit finite volume discretization which is solved both central in time and space.

$$\left(\frac{-k\Delta t}{\Delta x^2}\right)T_{n-1}^{i+1}+\left(\rho c_p+\frac{2k\Delta t}{\Delta x^2}\right)T_n^{i+1}+\left(\frac{-k\Delta t}{\Delta x^2}\right)T_{n+1}^{i+1}=\rho c_p T_n^i+e_n^{'}\Delta t \qquad (15)$$

Here k is the coefficient of heat conduction, Δt is the timestep size, Δx is the mesh element size (between adjacent nodes), ρ is the nodal mass density, c_p is the nodal heat capacity per unit mass in constant pressure, T is the temperature and e' is the heat generated per unit length of the resistant wires in the linear space domain. Superscripts denote the timestep and the subscripts denote the space variable.

$$r=\frac{k\Delta t}{\Delta x^2} \qquad (16)$$

$$\begin{bmatrix}1 & 0 & 0 & . & 0\\ -r & \rho c_p+2r & -r & . & .\\ 0 & -r & \rho c_p+2r & -r & 0\\ . & . & & . & \\ 0 & . & 0 & 0 & 1\end{bmatrix}\begin{Bmatrix}T_1\\ T_2\\ .\\ .\\ T_n\end{Bmatrix}^{i+1}=\begin{Bmatrix}\rho_1 c_{p1}T_1\\ \rho_2 c_{p2}T_2\\ .\\ .\\ \rho_n c_{pn}T_n\end{Bmatrix}^{i}+\Delta t\begin{Bmatrix}e_1'\\ e_2'\\ .\\ .\\ e_n'\end{Bmatrix} \qquad (17)$$

3. Results and Discussion

As a result of the analytical model solution, a resistant wire temperature exposure vs Fuel-Oil boiling point dependance chart has formerly been produced by the author. The possibility of boiling in the fuel carrying pipes can be taken into account for evaluating the gas + liquid Fuel-Oil entrance to the heater which is also an unwanted situation [7].

For generating the numerical scenario results, the fuel viscosity (μ)—so the pumping ability (*% mass flowrate*), thermostat reliability (a measure of correct value reading from the contacting and surrounding media), the thermostat reaction delay (t_{delay}), fuel flowrate and the fuel inlet temperature at initial conditions ($T_{in(t=0)} = T_{fuel\text{-}inlet}$) have been chosen as the main simulation parameters.

The numerical results have shown that, the temperature overgain may not majorly be affected by the fuel boiling point nor the fuel viscosity at the pump's gears. It can also be stated that, fuel flowrate was also not a major parameter affecting the heating behavior (mean temperature at the outlet of the heater) but it affected the effective heater power and the heater efficiency.

In the contrary, the effect of the thermostat reliability and the reaction time to read the correct value (t_{delay}) can barely be underlined as the main safety control parameters for the resistant wires.

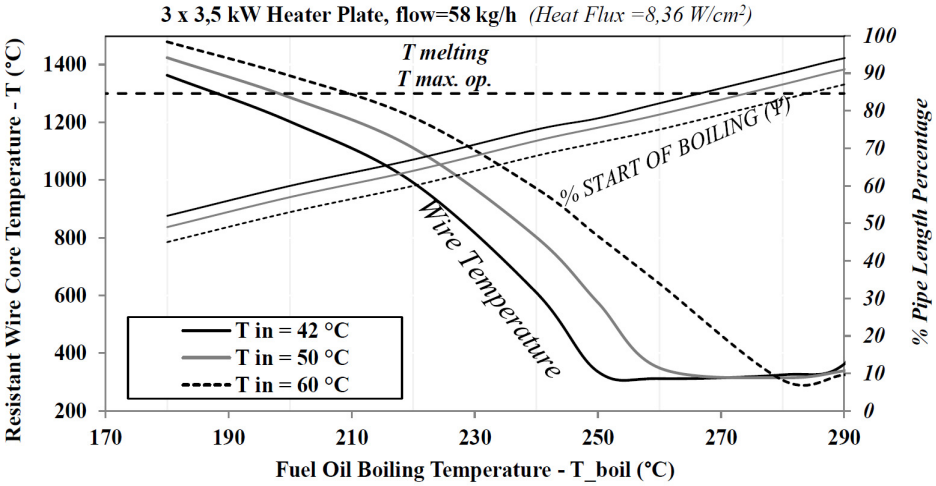

Fig. 6 Heater resistant wires' temperature exposure in case of boiling/multiphase flow [7].

The following results consist of:

• Time dependent temperature distribution curves with the last time step result in bold black line (top left);

• The sum of total power used for increasing the fuel internal energy from the inlet to the outlet and the power used for heating the inner space of the heater assembly (top right);

• Thermostat sensed temperature with the mean outlet temperature of the fluid fuel (bottom left);

• The power used for only increasing the fuel internal energy from inlet to the outlet (effective power) (bottom right).

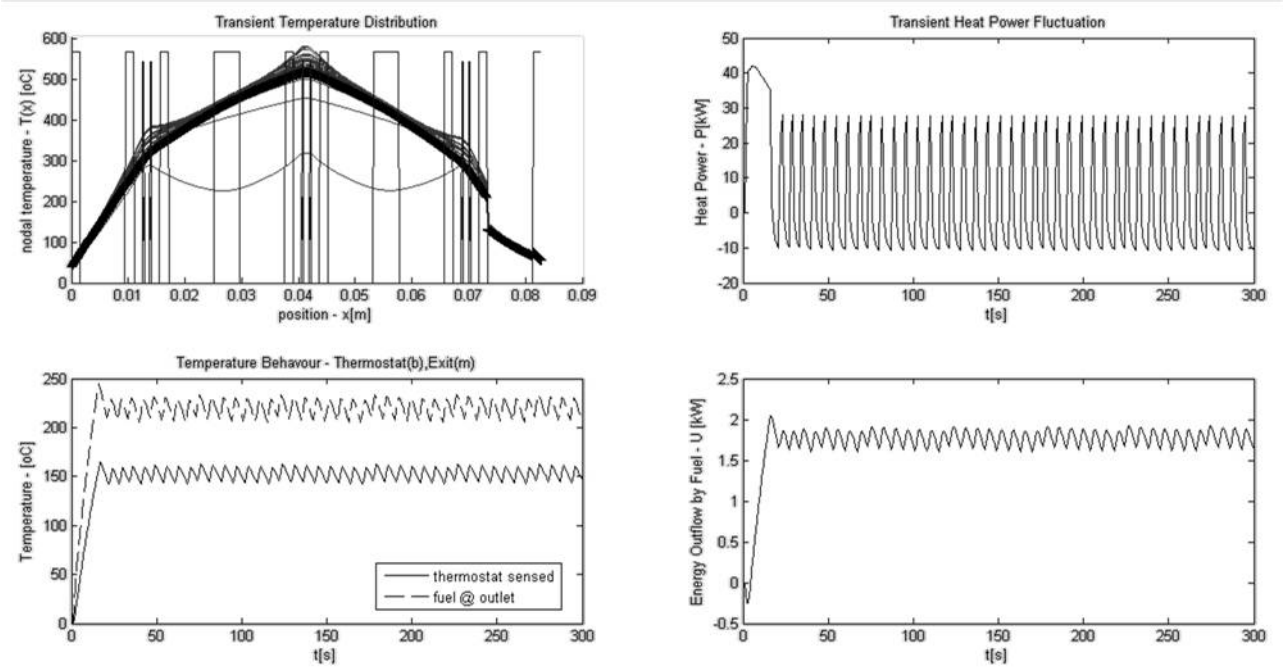

Fig. 7 Simulation results, t_{delay}=1s, N_p=3, $T_{fuel\text{-}inlet}$=42 °C, flow=58 kg/h, $T_{thermostat\text{-}set}$=150 °C, rms($U$)=1.7 kW [7].

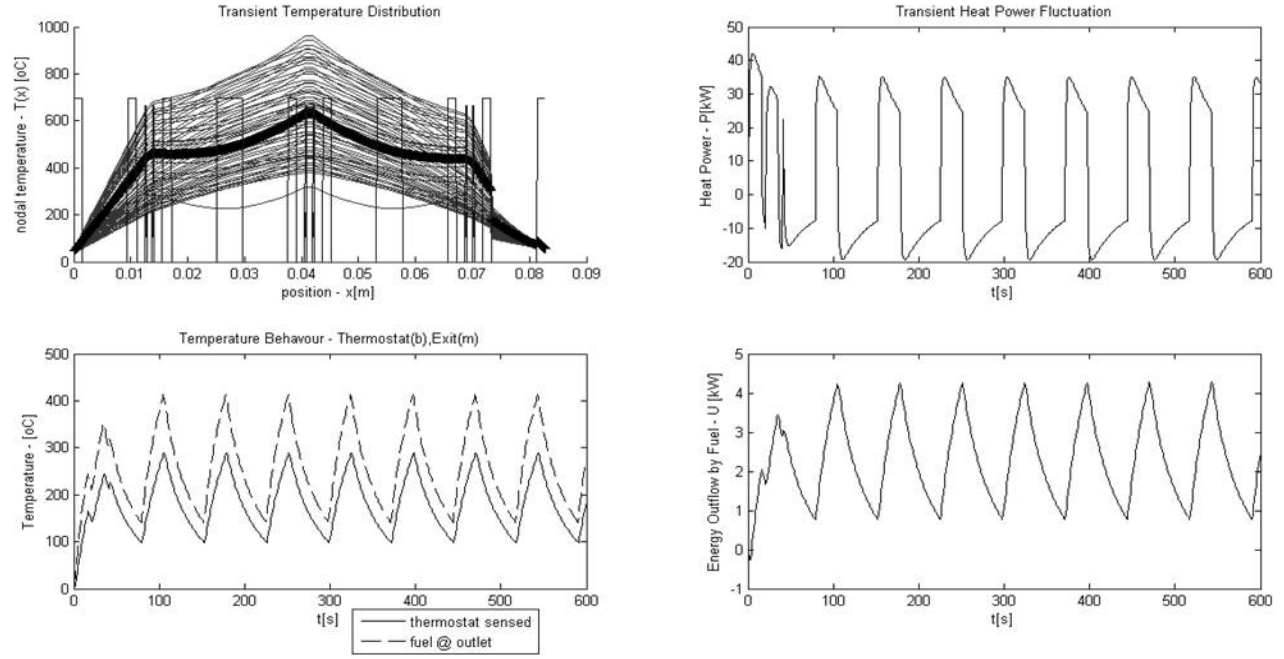

Fig. 8 Simulation results, N_p=3, t_{delay}=20 s, $T_{fuel\text{-}inlet}$=42 °C, flow=58 kg/h, $T_{thermostat\text{-}set}$=150 °C, rms($U$)=1.7 kW [7].

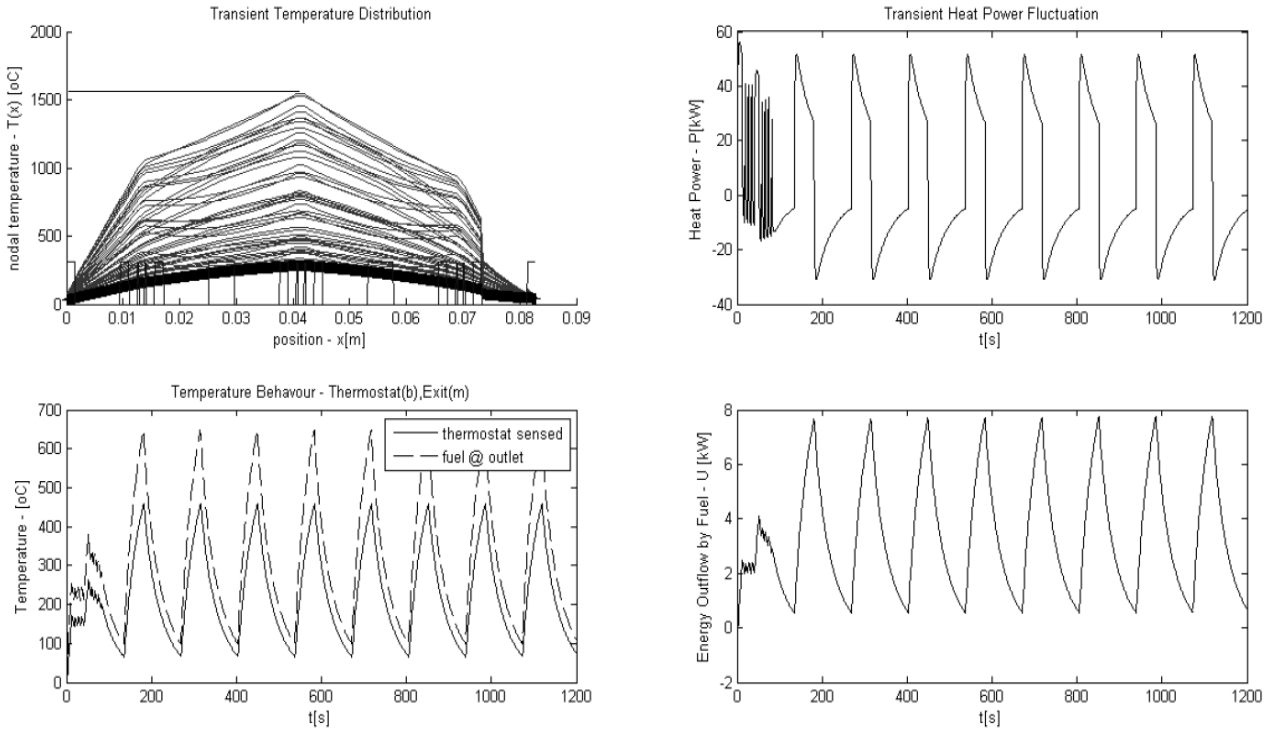

Fig. 9 Intolerable thermostat delay simulation results, N_p=3, t_{delay}=40 s, $T_{fuel\text{-}inlet}$=42 °C, flow=58 kg/h, $T_{thermostat\text{-}set}$=150 °C, rms($U$)=0.68 kW, mid-plates' temperature exceeds the maximum operational limit of 1,300 °C [7].

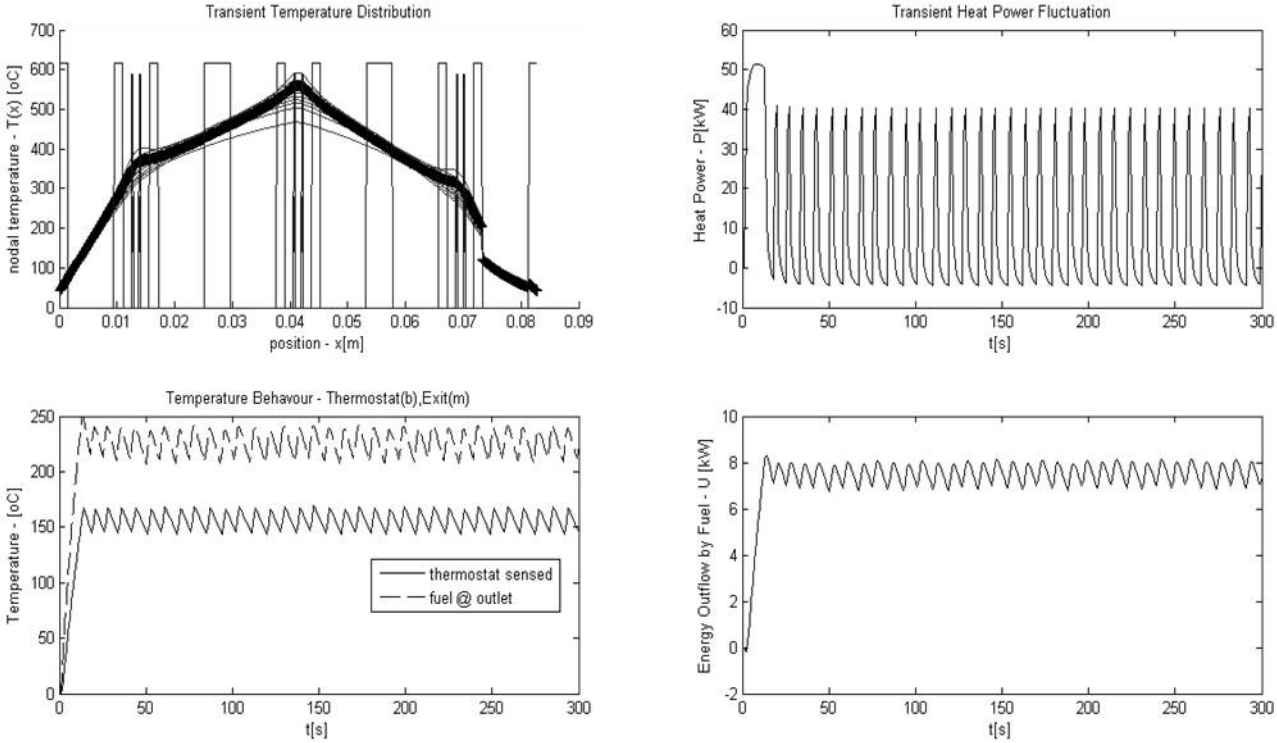

Fig. 10 Simulation results, N_p=3, t_{delay}=1 s, $T_{fuel\text{-}inlet}$=42 °C, flow=180 kg/h, $T_{thermostat\text{-}set}$=150 °C, rms($U$)=7.35 kW [7].

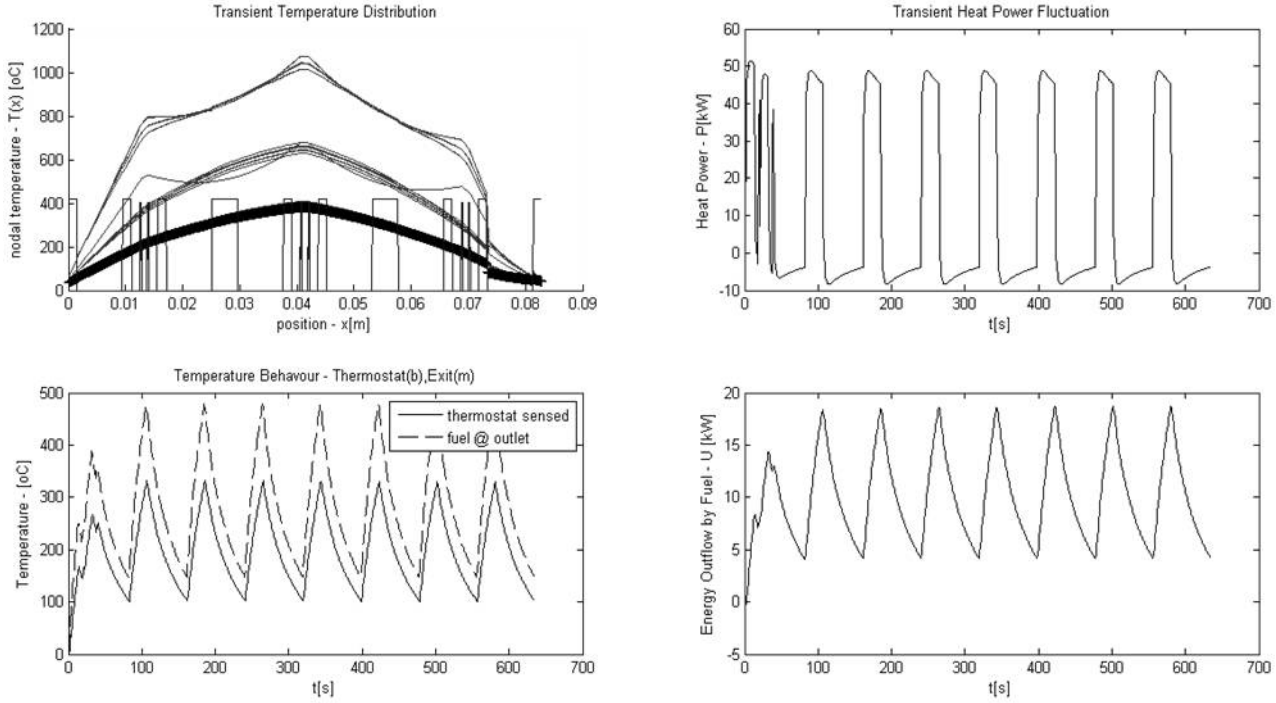

Fig. 11 Simulation results, N_p=3, t_{delay}=20 s, $T_{fuel\text{-}inlet}$=42 °C, flow=180 kg/h, $T_{thermostat\text{-}set}$=150 °C, rms($U$)=4.13 kW [7].

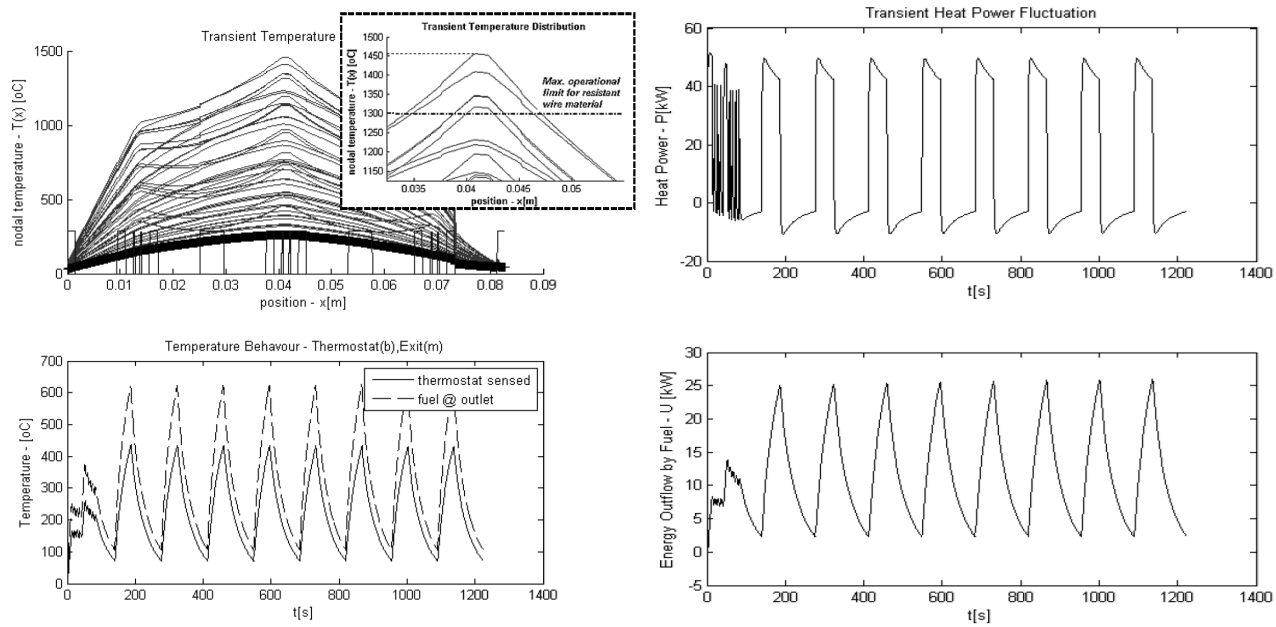

Fig. 12 Intolerable thermostat delay simulation results, N_p=3, t_{delay}=40 s, $T_{fuel\text{-}inlet}$=42 °C, flow=180 kg/h, $T_{thermostat\text{-}set}$=150 °C, rms($U$)=4.71 kW, mid-plates' temperature exceeds the maximum operational limit of 1,300 °C [7].

3.1 Numerical Solution with 58 kg/h Flowrate

The heater efficiency has been measured depending on previous quality control tests and has been stated earlier as 74% [14].

The effective power is a time series data so that, the mean value has been written by taking the rms value of the series below each graph set.

3.2 Numerical Solution with 180 kg/h Flowrate

The limiting thermostat behavioral effect on resistant wires' safe operation has been formerly declared by

the author as seen in Fig. 13 and Fig. 14.

The heat transferred to the flowing Fuel-Oil in a unit time has been plotted vs time and by taking the rms values of the time series data, the resultant calculated effective heat power values depending on the thermostat delay behavior were plotted in the previous and current graphs occupying Eq. (18).

$$\eta_t = \frac{\dot{m} c_v \left(T_{out} - T_{in}\right)}{10.5[kW]} x100 \qquad (18)$$

The heater thermal efficiency is calculated as follows and efficiencies at various important operating points are denoted in Fig. 13.

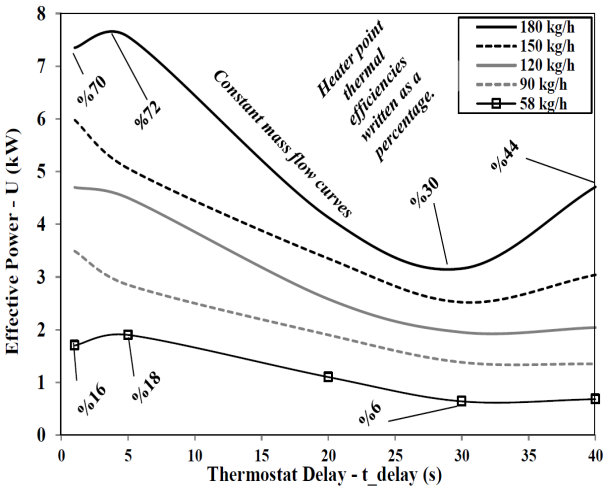

Fig. 13 Heater effective power vs thermostat delay for different fuel flowrates [7].

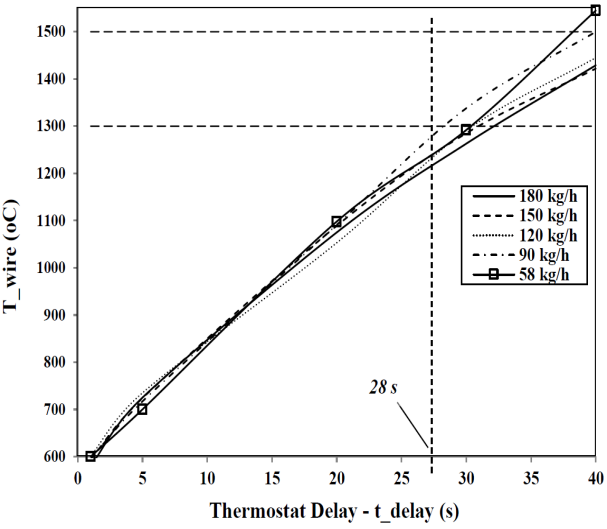

Fig. 14 Wires' maximum temperature of exposure vs thermostat delay [7].

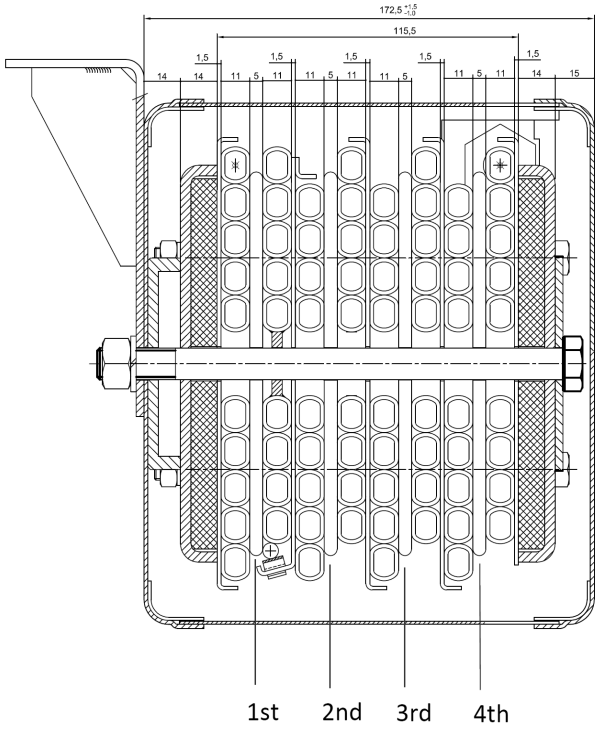

Fig. 15 N_p= 4 pre-heater assembly detail top section view.

3.3 Distributed and Reduced Heat Flux with Four Heater Plates

The introduced heater assembly with three heater plates has been issued as unreliable by means of overheating due to limiting thermostat sensing overdelay behavior with reference to the earlier results [7].

With the same resistance wire thickness (0.3 mm) and width (2.5 mm) a revised design has been implemented with an increased number of winding turns per plate, reducing the plate heat power from 3.5 kW to 2.6 kW (conserving the total heat power of 10.5 kW) has been regarded as a precaution in order to increase resistance to overheating, thus a wire rupture. The below results are generated by using the in-house MATLAB® code with number of plates N_p = 4 and wire produced heat flux of 28.3 kW/m^2.

Focusing attention on the peak temperature values displayed in the 3D plots in Fig. 16, it can be noticed that, the system temperature distribution oscillates with respect to time of every point on the geometrical span. There is no evidence for overheating like in the three plate version. The difference of fuel flowrate has

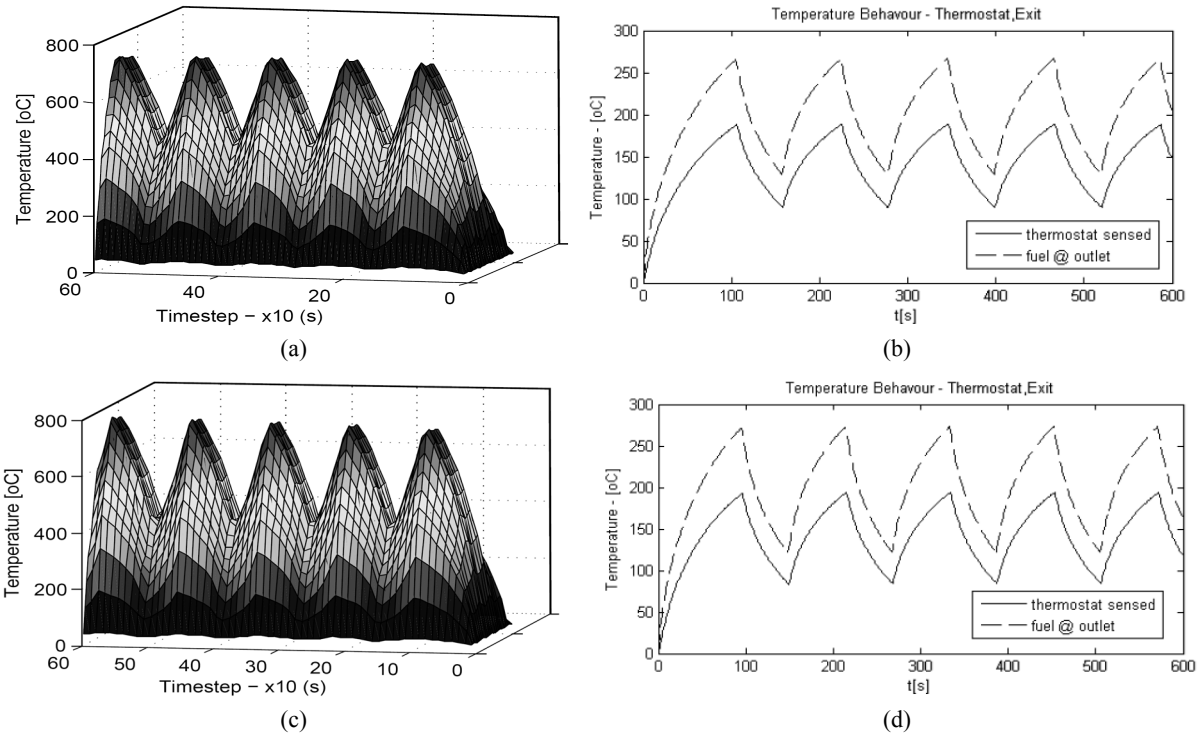

Fig. 16 Simulation results, $N_p = 4$, $t_{delay} = 40$s, $T_{fuel\text{-}inlet} = 42\ ^oC$, rms($U$) ≈ 10.5 kW for both results, flow = 180 kg/h (a, b), flow = 58 kg/h (c, d).

a negligible effect on the inner heating/cooling behavior. The maximum resistant wire temperatures will be no more than 800 ^oC which means a safe operation.

4. Conclusions

It is obvious that the heater operates in its most efficient state (72%) in case of maximum fuel flowrate with a quick responding thermostat. High speed response of the thermostat will keep the heater in its highest efficient operating range for any constant mass flowrate. Independent of the fuel flowrate, both the effective power and the heater wires' exposed temperature values show that, the thermostat can respond no later than 28 seconds for three plate formation. Thus the worst and least efficient operation occurs at this delay value.

Thermostat delay which is more than 28 seconds will also force the system to operate in the unsafe region ($T \geq 1{,}300\ ^oC$). The overdelay in thermostat operation for sensing the correct temperature can be counted as the main reason for the heater resistant wires' rupture phenomenon.

The increment in the Fuel-Oil burner's pre-heater has given enormously safe results when compared with the same flow + thermodynamic operation cases with three heater plates. This result can barely be concluded: as more the discretization of a heat pump and distribution to smaller, less the unused heat and rupture probability.

As a future work, the in-house heat transfer code is planned to be expanded to a 3D solver also including the solution for the flowfield. The safe operation cases and the related validation calculations are also in a close relation with exergy analysis such that, further exergy analyses for petroleum product fuels primarily focusing on the Fuel-Oil pre-heaters can also be counted as a future goal.

Acknowledgement

The author's grateful thanks to Alper ATA and Mehmet ÖNSEL of Alarko Carrier R&D for sharing their valuable knowledge about fuel oil burners.

References

[1] Kanthal®. 2012. "Kanthal-D (Strip) Datasheet Updated 2012-06-20." Sandvik AB©, Hallstahammar, Sweden. Accessed July 15, 2016. http://www.kanthal.com/en/products/material-datasheets/strip/kanthal-d/.

[2] HESS Corporation. 2012. *Safety Data Sheet. Material Name: No. 4 Fuel Oil.* US Globally Harmonized System SDS No: 15054. Woodbridge, New Jersey, 5. Accessed July 15, 2016. http://www.hess.com/docs/us-safety-data-sheets/fuel-oil-no-4.

[3] Wang, Z., Hollebone, B. P., Fingas, M., Fieldhouse, B., Sigouin, L., Landriault, L., et al. 2003. *Characteristics of Spilled Oils, Fuels, and Petroleum Products: 1. Composition and Properties of Selected Oils. National Exposure Research Laboratory.* Office of Research and Development, United States Environmental Protection Agency report.

[4] American Petroleum Institute (API). 2004. *Robust Summary of Information on Heavy Fuel Oils*. USA, US EPA., 201-15368B.

[5] American Petroleum Institute (API), Petroleum HPV Testing Group. 2011. "Heavy Fuel Oils Category Analysis and Hazard Characterization." *Submitted to the US EPA. Consortium Registration, Interim Final Document.* 29: 201-16867A.

[6] Gilyazetdinov, L. P. 1991. *Calculation of the Latent Heat of Vaporisation of Petroleum Fractions.* New York, NY: Plenum Publishing Corporation.

[7] Elbüken, B. 2016. "Investigation of Resistant Wires' Rupture Phenomenon Used in Fuel-Oil Burner Pre-Heaters by Analytical and Numerical Results". XII. International HVAC+R and Sanitary Technology Symposium. Accessed March 31-April 2, 2016. http://www.ttmd.org.tr/symposium2016/book.pdf.

[8] Miskimins, W. K., Ahn, H. J., Kim, J. Y., Ryu, S., Jung, Y. S., and Choi, J. Y. 2014. "Synergistic anti-cancer effect of phenformin and oxamate." *PloS one* 9(1), e85576.

[9] Perry, R. H., Green, D. W., and Maloney, J. O. 1997. *Perry's Chemical Engineer's Handbook.* New York, NY: McGraw-Hill., ISBN 0-07-084941-5.

[10] SUNTEC Insight®. 2013. "Oil Pump Type E 1001, Gear Sizes 4-6-7." Accessed September 13, 2013. http://www.suntec.fr/document/docgenerale/PDFanglais/E1001gb.pdf.

[11] Curl, H. J., and O'Donnell, K. 1977. *Chemical and Physical Properties of Refined Petroleum Products.* NOAA Technical Memorandum ERL MESA-17. Marine Ecosystems Analysis Program. NOAA Environmental Research Laboratories, Boulder, Colorado. US Dept. Of Commerce.

[12] VDI-Verlag GmbH. 1974. *VDI-WARMETLAS, Berechnungsblatter für den Warmeübergang. Verlag des Vereins Deutscher Ingenieure – Düsseldorf.* German., ISBN 3-18-400211-X.

[13] White, F. M. 1991. *Viscous Fluid Flow.* New York, NY: McGraw-Hill., ISBN 0-07-069712-4.

[14] Cengel, Y. A., and Ghajar, A. J. 2011. *Heat and Mass Transfer: Fundamentals & Applications*, New York, NY: McGraw-Hill.

[15] Patankar, S. V. 1980. *Numerical Heat Transfer and Fluid Flow*. New York, NY: Taylor & Francis, 0-89116-522-3.